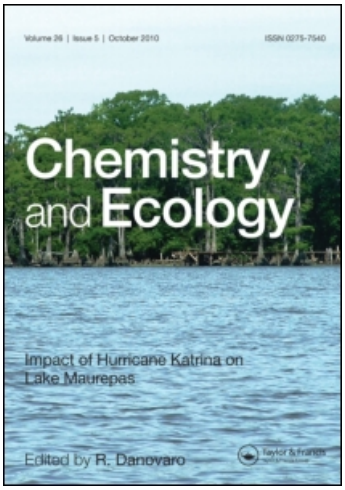

Chemistry and Ecology
Publication details, including instructions for authors and subscription information:
http://www.informaworld.com/smpp/title~content=t713455114

Recognition of water masses according to geochemical signatures in the Central Mediterranean sea: Y/Ho ratio and rare earth element behaviour

P. Censi[ab]; P. Zuddas[c]; D. Larocca[b]; F. Saiano[d]; F. Placenti[b]; A. Bonanno[b]
[a] Department CFTA, University of Palermo, Palermo, Italy [b] IAMC-CNR—Mazara del Vallo (TP) Via L. Vaccara, Mazara del Vallo, Italy [c] Institut de Physique du Globe de Paris, Paris, France [d] Department ITAF, University of Palermo, Palermo, Italy

To cite this Article Censi, P. , Zuddas, P. , Larocca, D. , Saiano, F. , Placenti, F. and Bonanno, A.(2007) 'Recognition of water masses according to geochemical signatures in the Central Mediterranean sea: Y/Ho ratio and rare earth element behaviour', Chemistry and Ecology, 23: 2, 139 — 153
To link to this Article: DOI: 10.1080/02757540701197879
URL: http://dx.doi.org/10.1080/02757540701197879

Chemistry and Ecology
Vol. 23, No. 2, April 2007, 139–155

Taylor & Francis
Taylor & Francis Group

Recognition of water masses according to geochemical signatures in the Central Mediterranean sea: Y/Ho ratio and rare earth element behaviour

P. CENSI*†‡, P. ZUDDAS§ , D. LAROCCA‡, F. SAIANO¶,
F. PLACENTI‡ and A. BONANNO‡

†Department CFTA, University of Palermo, Via Archirafi, 36-90123 Palermo, Italy
‡IAMC-CNR – Mazara del Vallo (TP) Via L. Vaccara, 61 91026 Mazara del Vallo, Italy
§Institut de Physique du Globe de Paris, 4, Place Jussieu, 75005 Paris, France
¶Department ITAF, University of Palermo, Viale delle Scienze, 13 90100 Palermo, Italy

(Received 25 July 2006; in final form 4 December 2006)

This study reports the results of geochemical investigations carried out in the Strait of Sicily (Central Mediterranean Sea) during the oceanographic cruise BANSIC 2000, focusing on the area around the Pantelleria Island. We evaluate the interface processes between dissolved phase and suspended particulate matter in the water columns on the basis of Y/Ho ratio and rare earth elements and yttrium distributions that are suitable to trace the occurrence of different water layers in Central Mediterranean Area. The main source of trace elements to the sea water system was recognized in the atmospheric fallout, while different scavenging mechanisms among Y and rare earth elements occur. Cation exchange at the dissolved phase–suspended media interface is driven by their external electronic configurations as monitored through the Y/Ho ratios, shape, and amplitude of the tetrad effects calculated along the water columns. The shape and amplitude of the tetrad effects in bottom waters suggest that the preferential Y scavenging from deep water layers depends on the hydrothermal activity in the seafloor. Here, Y is surface-complexed through the formation of inner-sphere complexes; Ho and other heavy rare earth elements are sorbed onto suspended particulate matter surfaces as weak outer-sphere complexes; these materials have a montmorillonite like nature; and preferential incorporation medium rare earth elements in crystal structures of biogenic carbonates is suggested by the relationship between the Eu anomaly and the nutrient contents of water masses.

Keywords: Rare earth elements; Tetrad effect; Y/Ho ratio; biogenic carbonates; Central Mediterranean

1. Introduction

The distribution of rare earth elements and yttrium (REY) in sea water allowed several researchers in the last 25 yr, to carry out interesting studies to:

(1) recognize fractionation processes between dissolved and suspended phases [1–4];

*Corresponding author. Email: censi@irma.pa.cnr.it

Chemistry and Ecology
ISSN 0275-7540 print/ISSN 1029-0370 online © 2007 Taylor & Francis
http://www.tandf.co.uk/journals
DOI: 10.1080/02757540701197879

(2) examine the capability of REY to depict evidence of anthropogenic input in river and coastal waters, with a special emphasis on countries surrounded by highly populated areas [5];
(3) evaluate the mechanisms of input of these elements in the sea-water system for atmospheric or riverine loads [6–8].

In the Mediterranean Sea, these studies have been poorly developed and have focused especially on the distribution of heavy metals in highly populated areas [9, 10]. In the stategic area of the strait of Sicily, only the water mass exchange between the eastern and western basin was investigated. In addition, it has been partially investigated during the European Community EROS program, with only a few studies on REY distributions along the water column [11] having been carried out. Few papers investigate rare earth element (REE) distributions in the Mediterranean System, in western [12, 13] and eastern basins [14–16] as a powerful geochemical tool to evaluate solid-water chemical exchange processes and complexation phenomena [1, 17]. REY distributions have a large interest to investigate occurrences of hydrothermal submarine activities that can be represented in the Strait of Sicily due to its geological context. The Strait of Sicily is a submarine continental rift formed by transtensional tectonics which have affected the northern margin of the African plate since the Late Miocene, in response to the opening of the Tyrrhenian Sea and a differential anti-clockwise rotation of Sicily with respect to Africa [18–20]. The rift system is marked by a series of en-echelon axial grabens, trending N120°, widening to the south-east, and ranging in depths. This is a very interesting area in which active volcanism and tectonically related thermal processes occur in the Pantelleria area and can occur also in the surrounding seafloor [21].

Therefore, several extensive oceanographic cruises have been carried out in this previously poorly studied area [7, 22] with a particular emphasis on filling the gaps of knowledge in this area.

The aims of this research are:

(1) to evaluate the capability of REY to track the different water masses in the Strait of Sicily, with special emphasis on the westward flow of Levantine Intermediate Water (LIW) and the Eastern Mediterranean Deep Water (EMDW) through this area;
(2) to recognize the effects of solution complexation–surface complexation processes as drivers of REY distributions in the different components of water masses,
(3) to evaluate the possible occurrence of seafloor thermal activity close to Pantelleria Island, on the basis of the modifications of geochemical characters of the bottom water masses induced by external inputs suitable for inducing variations in Y/Ho ratio values and shale-normalized REY behaviour in dissolved media and suspended particulate matter (SPM).

2. Material and methods

2.1 *Studied area*

Sea water was collected from six sampling stations along the central area of the Strait of Sicily in the early summer of 2000 during the BANSIC 2000 oceanographic cruise, aboard the RV *Urania* (figure 1).

The sampling system consisted of a Neil-Brown CTD rosette frame and 24×12 l Teflon-lined GoFlo bottles. Upon recovery of the GoFlo bottles, water samples were immediately

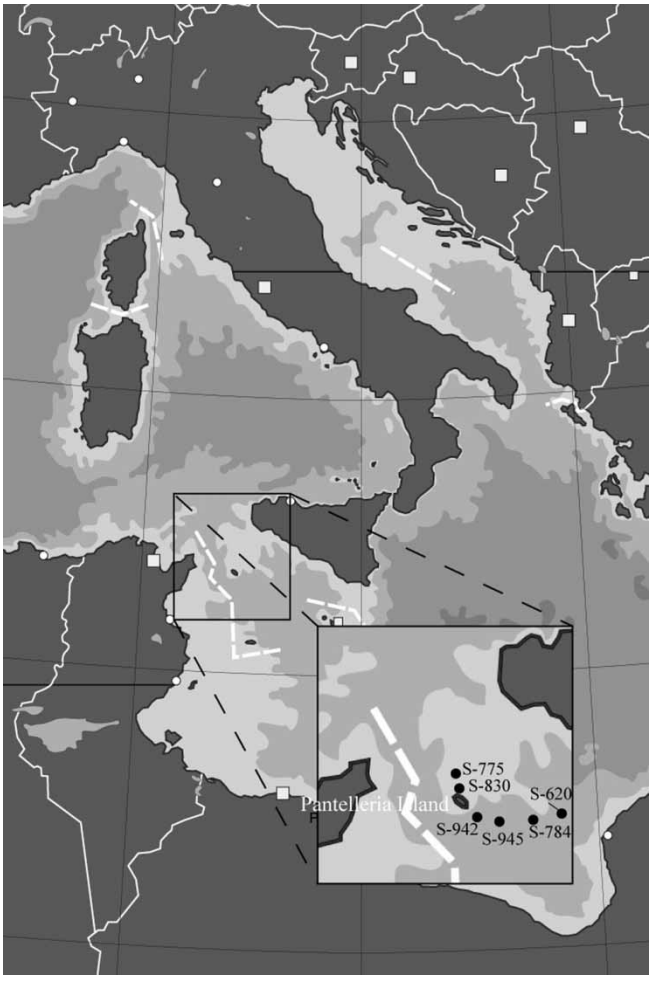

Figure 1. Location of the sampling sites and study area.

filtered inside the shipboard through 0.2-μm Millipore® filters (using Teflon tubing apparatus, in order to avoid dissolution of labile particulate fraction [23]) and then acidified to pH 1–2 with HNO_3 Merck ULTRAPUR®. All the water samples were treated under a laminar air flow clean bench to minimize contamination, and the sampling materials were cleaned with high-purity-grade reagents (Merck ULTRAPUR®).

2.2 *Dissolved phase*

In order to increase the signal/noise ratio in the studied sea waters, 1000 ml of each sample was pre-concentrated with CHELEX 100® (200–400 mesh) chelating resin:

- The pH of each sea-water sample was set to 6.0 with CH_3COONH_4 [24], and each sea-water sample was passed along a 8-cm-long column filled with CHELEX-100 previously cleaned

and conditioned [25], using a Supelco™ 12 visiprep SPE vacuum manifold equipped with 12 polypropilene columns (12 mL in volume).
- REE were eluted with 5 ml of HNO_3 3.5 M, giving a 200-fold enrichment factor. Details of the used procedures are reported in Möller *et al.* [24] and Paulson [25].

REY recoveries were monitored using two artificially prepared sea-water standard solutions at 1 $\mu g\,l^{-1}$ and 20 $\mu g\,l^{-1}$ and ranging from 94.89% and 99.89% for Y and Tm, respectively. For precision and accuracy see Censi *et al.* [7, 8].

The eluted fractions were analysed with a high-resolution ICP-MS Finnigan Element 2 from the University of Catania using 100 $ng\,l^{-1}$ Rh as an internal standard. The measurements were carried out in high-resolution mode, allowing the signal of the elements to be separated from those of most isobaric interferences as BaO^+. Analytical blanks were obtained with 50 ml of HNO_3 Merck ultrapure in Millipore ultrapure waters, and their concentrations were negligible compared with the measured REE concentrations. All methodologies were carried out as extensively described in previous publications [7, 8, 26].

2.3 *Suspended particulate matter*

Particulate matter was collected on a Millipore® filter from sea water (approximately 6 l). After weighing with a ±0.01 mg analytical balance, the recovered fractions were digested as reported previously [7] using a microwave oven CEM® Mars 5 equipped with TFM® vessels to which an acid solution had been added, with proportions HCl:HNO_3:HF=4:4:4 (total volume=12 ml). The containers were accurately sealed, put into the carousel, and heated with 100% power (1200 W), with a pressure ramp of 30 min, and then maintained at a constant pressure (2.76 MPa) and temperature (220 °C) for 2 h.

After complete dissolution, the acid excess was removed up to incipient dryness using a microvap™ apparatus, and 5 ml of nitric acid (65 % v/v) was added. The sample solutions were then diluted to 100 ml with Millipore® water and transferred into clean 100-ml polycarbonate bottles. The obtained solutions were directly analysed after 1:50 dilution with 5% HNO_3 Merck ULTRAPUR® solution adding 100 $ng\,l^{-1}$ Rh solution as internal standard.

3. Results

The distribution of REY has been investigated in dissolved phase and suspended particulate matter from the water masses of the Strait of Sicily. This investigation was carried out through a detailed NW–SE sampling approach to follow the geological structures in the seafloor and to investigate the vertical distributions of trace elements along the water columns. The dissolved REY concentrations at the seven stations together with the main hydrographic parameters (potential temperature and salinity) and geographical locations are listed in table 1, and the REY concentrations in SPM are given in table 2.

Because of the presence of hydrothermal activity around the Pantelleria Island, the oceanographic investigations were carried out in the deepest area of the Strait of Sicily, close to the island, to recognize occurrences of a 'crustal contribution' on the basis of the features of REE and yttrium shale-normalized concentrations. The REE normalized concentrations, $[REE_i^{SN}]$, were calculated according to the expressions:

$$[REE_i^{SN}] = \frac{[REE_i^{sample}]}{[REE_i^{PAAS}]},$$

Table 1. Sampling location, depth (m), and REY contents (pmol l^{-1}) studied in the dissolved phase.

	Longitude	Latitude	Depth	Salinity	Fluorometry	Y	La	Ce	Pr	Nd	Sm	Eu	Gd	Tb	Dy	Ho	Er	Tm	Yb	Lu
S-620	13° 11.695	36° 38.687	10	37.56	0.09	236.27	29.31	11.06	3.61	20.24	3.59	0.97	4.16	0.80	8.49	2.45	5.44	1.28	8.93	1.41
			30	37.60	0.08	228.25	20.48	13.48	3.45	17.40	4.07	1.05	3.63	0.78	8.15	2.44	6.07	1.02	7.25	1.16
			200	38.70	0.09	204.56	22.93	15.20	3.76	22.40	4.31	1.17	5.67	1.27	9.57	2.28	6.86	0.97	7.24	1.20
S-775	12° 12.095	36° 52.294	26	37.25	0.18	160.85	22.15	13.58	3.66	18.36	3.76	0.96	3.77	0.78	6.41	1.76	6.26	1.13	7.31	1.08
			40	37.31	0.23	196.98	21.84	8.61	3.39	20.23	4.10	0.73	3.86	0.86	7.36	2.08	6.42	1.06	7.52	1.20
			180	38.72	0.15	195.00	21.53	14.89	3.80	23.12	4.23	1.08	4.13	0.96	8.53	2.17	6.40	1.11	7.55	1.16
			800	38.78	0.04	187.88	22.50	13.56	4.70	15.87	3.99	0.52	3.86	0.98	8.64	2.33	7.04	1.09	7.74	1.24
S-784	12° 50.991	36° 34.294	25	37.51	0.36	225.64	25.72	9.98	3.54	19.23	4.46	0.57	4.20	1.00	8.77	2.27	6.01	1.06	7.26	1.13
			40	37.52	0.20	199.26	23.28	14.67	3.64	19.77	4.60	0.81	4.07	0.72	7.36	2.14	7.79	1.11	6.68	0.91
			90	38.06	1.33	232.49	22.65	8.99	3.73	18.08	3.42	1.01	4.13	0.87	8.87	2.43	7.35	1.24	8.25	1.24
			145	38.61	0.17	182.56	21.85	10.62	3.20	18.05	5.60	0.42	2.83	0.86	7.33	1.96	8.14	1.39	9.49	1.47
			500	38.76	0.13	137.18	27.90	10.50	3.82	16.03	3.07	1.00	3.95	1.00	8.18	2.03	6.33	1.01	7.02	1.10
			710	38.77	0.22	160.18	24.35	13.78	2.91	18.48	4.48	0.71	4.59	0.87	8.32	2.25	7.44	1.28	8.48	1.27
			920	38.78	0.14	176.77	22.90	11.13	4.02	18.28	4.61	1.07	5.03	1.12	8.69	2.30	7.26	1.20	8.23	1.28
S-830	12° 9.5485	36° 48.830	19	37.23	0.18	211.06	33.29	16.38	2.81	19.25	3.99	0.71	4.31	0.99	10.24	2.32	7.27	1.12	7.73	1.21
			50	37.29	0.43	217.98	23.38	8.86	3.54	14.93	4.93	0.51	2.95	0.57	7.24	2.29	8.96	1.42	9.54	1.45
			130	38.23	0.76	173.94	22.74	14.28	4.70	19.76	3.76	0.39	3.85	0.95	6.88	1.79	6.18	1.07	7.74	1.25
			605	38.76	0.14	164.21	23.52	9.78	3.65	19.37	4.77	0.80	5.23	1.07	7.67	2.18	6.92	1.14	7.77	1.20
			860	38.77	0.14	171.56	28.82	16.45	4.84	18.46	3.20	0.62	5.18	0.88	7.35	2.09	7.27	1.00	7.05	1.12
			1100	38.75	0.16	153.38	22.62	10.27	4.79	16.84	3.50	0.72	3.97	0.99	7.67	2.11	6.71	1.18	7.92	1.20
S-942	12° 4.4596	36° 41.902	10	37.28	0.17	223.05	31.38	13.65	3.02	16.90	3.76	0.77	4.18	0.93	9.69	2.21	6.86	0.99	6.39	0.94
			25	37.20	0.20	221.08	25.32	16.11	3.22	19.39	4.35	0.62	3.73	0.92	7.85	2.31	8.84	1.37	8.90	1.31
			50	37.21	0.28	225.64	22.54	10.28	3.50	15.94	3.20	0.49	4.00	0.73	8.02	2.43	9.23	1.20	9.06	1.52
			100	37.86	0.65	201.10	29.71	18.62	2.93	16.20	3.90	0.42	3.53	0.92	7.79	2.06	7.07	0.95	6.39	0.98
			515	38.77	0.30	156.29	27.19	16.17	3.12	18.04	4.49	0.90	4.18	0.80	8.24	2.21	6.92	1.09	8.03	1.32
			700	38.77	0.33	166.82	23.92	12.06	4.10	16.70	3.12	0.51	3.69	0.68	8.14	2.09	7.52	1.15	8.12	1.30
S-945	12° 17.412	36° 35.902	10	37.26	0.16	194.72	25.09	8.00	3.90	16.70	3.29	1.00	4.90	0.95	8.29	1.98	9.23	1.43	9.77	1.51
			25	37.27	0.17	215.48	23.98	8.80	3.55	20.80	4.09	0.72	4.12	0.91	7.72	2.25	7.17	1.16	7.82	1.20
			50	37.31	0.22	171.16	23.45	12.87	3.55	17.33	4.26	0.62	3.77	0.69	6.41	1.92	6.46	1.04	7.36	1.18
			200	38.74	0.15	235.49	30.00	12.94	4.50	27.73	4.23	0.87	4.19	0.75	8.53	2.43	8.14	1.51	9.95	1.49
			465	38.77	0.43	198.31	23.81	13.59	3.99	22.21	4.43	0.79	4.13	0.96	8.17	2.13	7.14	1.21	8.39	1.32
			605	38.76	0.03	137.18	24.89	13.71	3.37	17.36	4.29	0.61	4.26	1.01	8.81	2.11	6.97	1.10	7.51	1.16
			805	38.75	0.24	173.94	24.90	10.71	3.55	17.33	3.87	0.98	5.03	1.06	7.19	1.92	6.38	1.10	7.78	1.24
			1000	38.75	0.13	150.80	23.90	9.00	3.55	15.35	4.56	0.78	4.78	0.84	6.37	1.81	7.08	1.28	8.74	1.35
			1255	38.75	0.14	171.68	23.76	14.27	4.51	16.87	4.23	0.70	4.87	0.83	7.99	2.16	7.04	1.15	8.57	1.43

Table 2. Sampling depth (m), Cd/Sc ratio, and REY contents ($\mu g\,kg^{-1}$) in the SPM samples studied.

	Depth	Cd/Sc	Y	La	Ce	Pr	Nd	Sm	Eu	Gd	Tb	Dy	Ho	Er	Tm	Yb	Lu
S-620	10	1.70	4.15	9.65	20.27	1.84	5.59	1.03	0.27	0.76	0.13	0.86	0.14	0.30	0.05	0.29	0.05
	30	1.50	3.79	9.22	27.97	2.22	6.03	0.76	0.24	0.65	0.10	0.60	0.11	0.30	0.05	0.26	0.05
	200	0.84	21.95	16.40	32.42	4.15	17.19	3.80	1.01	3.26	0.48	2.45	0.49	1.31	0.16	0.87	0.10
S-775	26		18.55	35.87	79.02	9.57	33.03	6.99	1.75	4.29	0.64	2.92	0.55	1.31	0.16	1.01	0.20
	40	1.20	4.23	9.88	25.99	3.16	9.14	1.23	0.33	0.89	0.10	0.73	0.13	0.31	0.05	0.28	0.05
	180	1.47	15.50	51.61	183.60	15.77	34.19	5.00	1.01	2.31	0.35	1.93	0.37	0.83	0.11	0.60	0.08
	800	1.39	23.41	77.79	92.22	9.32	25.80	4.95	1.50	4.60	0.71	2.60	0.51	1.32	0.21	1.27	0.15
S-784	25		3.82	25.99	109.78	10.42	29.47	3.84	0.54	0.75	0.10	0.58	0.13	0.36	0.05	0.37	0.06
	40	1.53	1.69	3.82	11.17	1.10	3.34	0.45	0.09	0.28	0.04	0.26	0.06	0.17	0.03	0.17	0.03
	90	1.56	5.55	31.24	108.62	9.66	29.24	2.57	0.35	0.69	0.11	0.78	0.18	0.48	0.07	0.51	0.08
	145	1.16	14.40	20.22	54.54	5.37	19.92	3.10	0.79	1.67	0.25	1.44	0.34	0.94	0.15	0.81	0.13
	500	0.35	4.06	8.81	20.00	2.62	8.70	1.64	0.40	0.80	0.09	0.42	0.07	0.16		0.13	0.02
	710	1.37	21.30	42.34	67.64	7.75	28.96	4.36	1.15	2.92	0.39	2.41	0.42	1.08	0.14	0.65	0.11
	920	1.08	22.82	31.24	88.08	8.12	28.45	4.84	0.92	2.28	0.39	2.13	0.37	0.86	0.08	0.38	0.06
S-830	19	0.83	8.10	34.74	67.61	5.76	22.70	3.05	0.43	0.82	0.14	0.91	0.28	0.79	0.17	1.21	0.15
	50	1.58	6.65	57.73	129.58	9.51	31.43	2.71	0.61	1.50	0.20	0.85	0.21	0.65	0.10	0.79	0.10
	130	1.91	9.58	16.97	47.84	6.51	22.61	3.19	0.75	1.96	0.26	1.32	0.26	0.59	0.07	0.36	0.05
	605	1.12	111.78	63.79	91.62	12.24	46.70	9.80	2.90	10.37	1.73	10.49	1.96	4.01	0.33	1.59	0.25
	860	0.15	44.50	34.68	48.74	5.52	26.16	4.62	1.25	3.56	0.62	3.30	0.67	1.72	0.20	1.15	0.14
	1100	1.28	7.54	14.28	38.70	2.47	6.60	1.22	0.21	0.59	0.08	0.50	0.11	0.30	0.04	0.17	0.03
S-942	10	1.07	9.29	19.50	52.09	2.68	9.31	1.79	0.36	0.72	0.12	1.03	0.26	0.92	0.16	1.15	0.16
	25	1.13	7.54	11.34	32.87	1.98	6.57	1.06	0.24	0.66	0.12	0.88	0.22	0.48	0.08	0.47	0.07
	50	0.65	13.69	49.43	119.33	4.42	16.26	3.09	0.84	2.26	0.25	1.87	0.47	1.35	0.21	1.31	0.23
	100	1.96	2.81	5.95	22.00	1.99	5.78	0.82	0.19	0.56	0.08	0.46	0.08	0.15	0.02	0.10	0.02
	515	1.55	7.39	8.83	17.80	1.88	5.39	0.99	0.24	0.73	0.11	0.63	0.14	0.38	0.05	0.28	0.04
	700	1.67	27.88	40.25	94.26	8.60	36.25	6.26	1.73	4.93	0.76	3.37	0.65	1.77	0.17	0.97	0.13
S-945	10	1.19	8.69	42.97	67.10	2.98	8.52	2.02	0.51	1.15	0.18	1.36	0.30	0.85	0.12	0.72	0.12
	25	0.80	7.64	33.86	63.13	3.40	11.76	2.14	0.41	0.77	0.13	0.93	0.23	0.75	0.13	0.72	0.13
	50	1.39	8.86	46.53	108.83	6.75	20.54	3.14	0.61	1.04	0.14	1.20	0.29	0.81	0.16	1.21	0.17
	200	1.24	11.92	13.36	42.79	4.25	16.68	2.67	0.87	2.66	0.41	1.99	0.30	0.70	0.09	0.46	0.06
	465	1.81	14.75	23.13	70.12	7.07	21.79	3.60	0.95	2.57	0.37	1.89	0.36	0.92	0.12	0.64	0.09
	605	0.03	29.74	31.22	35.89	4.54	17.63	4.17	1.15	3.74	0.61	3.11	0.61	1.31	0.12	0.60	0.09
	805	1.42	39.66	49.82	91.25	7.46	27.52	5.29	1.78	4.70	0.64	3.06	0.75	1.57	0.20	1.15	0.13
	1000	0.16	5.87	9.22	28.70	3.04	5.52	1.06	0.23	0.75	0.08	0.44	0.09	0.26	0.03	0.16	0.03
	1255	0.43	24.45	24.82	94.79	13.20	33.43	6.14	1.98	5.21	0.71	3.67	0.36	0.72	0.08	0.34	0.05

Table 3. Amount of REY released during sample treatments (PB).

	AB-1 pmol l^{-1}	AB-2 pmol l^{-1}	AB-3 pmol l^{-1}	AB-4 pmol l^{-1}	AB-5 pmol l^{-1}	Mean pmol l^{-1}	$\sigma\pm$ pmol l^{-1}	PB-1 pmol l^{-1}	PB-2 pmol l^{-1}	PB-3 pmol l^{-1}	PB-4 pmol l^{-1}	PB-5 pmol l^{-1}	L_c pmol l^{-1}	L_D pmol l^{-1}	L_Q pmol l^{-1}	EL-1 %	EL-2 %	EL-3 %	EL-4 %	EL-5 %	Mean %	$\sigma\pm$ %
Y	1.34	0.89	1.93	1.33	2.09	1.52	0.49	3.45	4.97	7.54	4.95	5.82	0.27	0.54	1.66	90.52	94.00	92.96	93.95	91.16	92.52	1.60
La	1.04	2.16	1.29	0.56	1.63	1.34	0.60	1.56	1.27	2.42	0.71	1.13	0.33	0.66	2.06	95.14	92.40	96.09	92.28	92.87	93.75	1.74
Ce	2.35	1.94	2.86	2.97	1.64	2.35	0.58	2.13	3.36	2.53	2.27	3.28	0.37	0.75	2.32	97.25	93.80	101.14	92.21	96.56	96.19	3.44
Pr	1.89	3.12	0.93	3.04	1.88	2.17	0.92	1.97	2.95	2.50	2.27	3.64	0.62	1.24	3.86	90.67	92.28	87.99	90.47	90.38	90.36	1.53
Nd	0.25	0.26	0.25	0.29	0.25	0.26	0.02	0.65	0.32	0.86	0.44	0.54	0.13	0.27	0.82	92.34	94.94	91.54	95.67	96.37	94.17	2.12
Sm	2.08	2.63	2.46	2.95	3.07	2.64	0.40	0.67	0.52	1.12	0.40	0.59	0.21	0.42	1.29	96.78	98.39	97.56	92.33	92.91	95.59	2.78
Eu	2.29	1.98	2.37	1.33	2.80	2.15	0.55	0.65	0.84	1.44	0.91	0.91	0.12	0.24	0.73	90.18	93.38	92.83	87.60	91.11	91.02	2.30
Gd	1.41	1.16	1.55	2.03	1.46	1.52	0.32	1.17	1.02	2.11	1.32	1.41	0.25	0.49	1.52	91.82	89.18	90.07	87.04	91.48	89.92	1.93
Tb	0.09	0.32	0.09	0.47	0.38	0.27	0.17	1.85	3.49	3.08	2.45	3.75	0.20	0.39	1.21	93.06	96.44	93.93	91.24	96.74	94.28	2.32
Dy	0.10	0.37	0.10	0.38	0.39	0.27	0.15	2.18	3.53	2.44	2.02	3.59	0.55	1.10	3.42	93.95	96.63	88.89	94.27	96.85	94.12	3.21
Ho	0.77	1.10	0.86	1.03	1.42	1.04	0.25	2.04	3.03	2.59	2.35	3.11	0.14	0.27	0.84	93.46	89.61	95.40	88.56	89.51	91.31	2.96
Er	0.26	0.30	0.28	0.25	0.31	0.28	0.03	1.93	3.13	2.67	2.00	3.03	0.45	0.90	2.78	91.40	86.90	90.60	90.82	82.21	88.38	3.88
Tm	1.93	2.78	2.44	3.49	3.34	2.80	0.64	1.72	3.57	2.73	2.16	3.77	0.42	0.85	2.63	92.30	95.19	94.52	90.25	96.40	93.73	2.45
Yb	2.27	1.75	2.59	1.62	2.98	2.24	0.57	1.71	3.34	3.05	2.15	2.95	0.19	0.39	1.21	93.22	98.53	98.67	95.14	91.43	95.40	3.20
Lu	0.09	0.34	0.09	0.40	0.39	0.26	0.16	2.16	3.21	3.06	2.08	3.51	0.48	0.96	2.98	94.47	93.85	89.87	89.28	95.36	92.57	2.79

Note: With these values, the calculation of critical values (L_c), detection limits (L_D), and limit of quantification (L_Q) for the used procedures was evaluated. EL-1÷EL-5 denotes the recovery measured for the analysed elements with ion-exchange resin.

where $[REE_i^{PAAS}]$ is the content of each REE in the Post Archean Australian Shales (PAAS) from Taylor and McLennan [27].

The evaluation of anomalous depletions or enrichments of selected REE in shale-normalized distribution can be expressed in terms of 'anomalies' defined as:

$$\frac{[REE_i]}{[REE_i]^*} = \frac{2^*[REE_i]_n}{[REE_{i-1}]_n + [REE_{i+1}]_n},$$

where $[REE_i]_n$ represents the normalized content of some REE, and $[REE_{i-1}]_n$ and $[REE_{i+1}]_n$ represent the REE contents of the previous and the next REE [2].

This information was collected and discussed in the light of the stratigraphy of investigated water masses, independently evaluated according to the recorded salinity values and four different water layers recognized: surface layer (0–50 m depth), first intermediate layer (50–200 m depth), second intermediate layer (200–800 m depth), and bottom water layer (down to 800 m depth). The behaviour of salinity along the water column can be seen as lower values are attained in the shallow waters; the salt contents slowly increase to 200 m depth and attain a maximum, close to 39% at about 400 m depth (table 1). Also, the REY behaviour along the water columns is evaluated in terms of the shale-normalized distributions (figure 2).

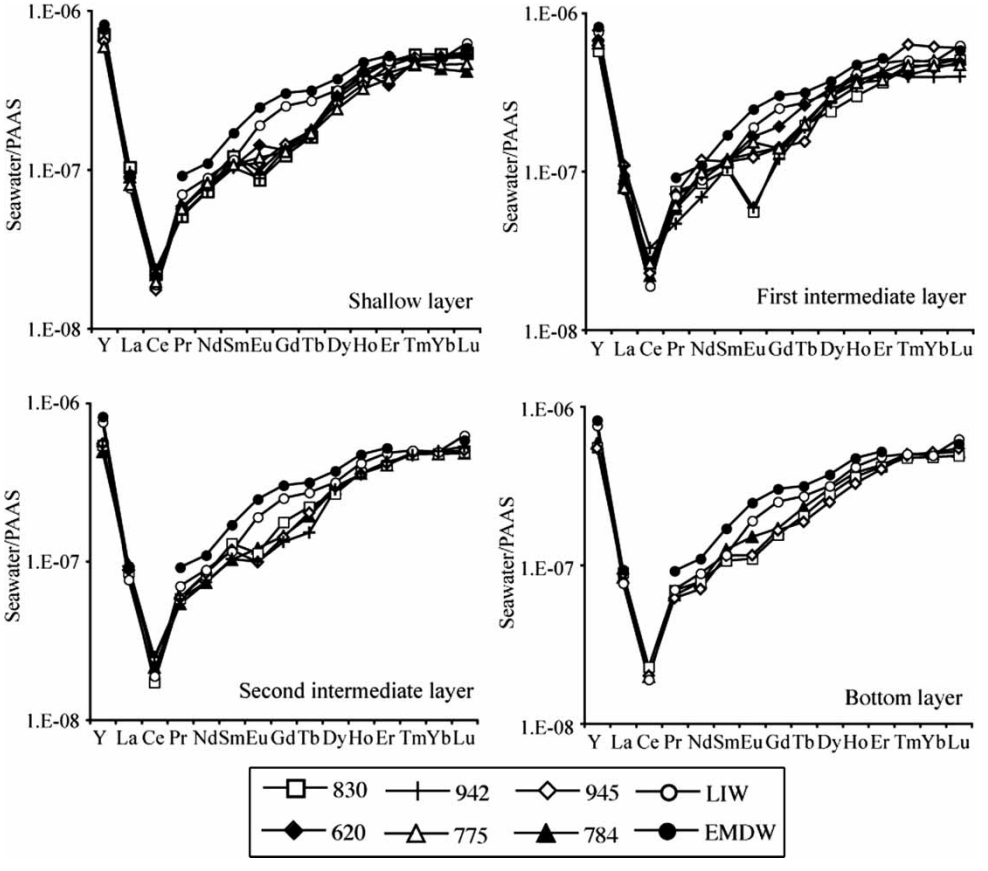

Figure 2. Shale-normalized REY patterns calculated for the average concentrations measured in the dissolved phase of the different water layers. Patterns of LIW and EMDW are given from Bau *et al.* [16].

3.1 *Dissolved phase*

3.1.1 Surface layer (0–50 m). The REE behaviour in surface waters show a negative Ce anomaly, typical of the sea-water environment, strong HREE enrichments with respect to LREE, and a negative Eu anomaly, which is larger in samples from the Pantelleria area (figure 2). Moreover surface waters from stations S-620, S-775, and S-784 show:

- a similar REE behaviour in terms of shale-normalized concentrations with differences among the several sampling sites only in terms of Eu concentrations;
- shale-normalized behaviours similar to those calculated for Eastern Mediterranean Deep Water (EMDW) and Levantine Intermediate Water (LIW) [16] in terms of light REE (LREE) and HREE contents, respectively;
- a medium REE depletion especially with regard to Eu and Gd in stations far from the Pantelleria area; and
- Stronger negative Eu anomalies, low Gd and Tb contents.

3.1.2 First intermediate layer (50–200 m). In the first intermediate water layer, immediately beneath the surface waters, the REE behaviour suggests a larger scattering of normalized Eu contents with negative anomalies larger than that reported for LIW, EMDW, and shallow waters (figure 2), while the Ce anomaly values are similar to those measured in different water layers.

The occurrence of strong Eu anomalies are well enhanced in shale-normalized distributions of 830 and 942 sampling sites, close to Pantelleria Island.

3.1.3 Second intermediate layer (200–800 m). In the 200–800 m depth layer, the shale-normalized pattern of the dissolved phase shows a moderate yttrium depletion and similar contents in LREE from the waters with respect to both LIW and EMDW, lower medium REE contents, from Sm to Dy (MREE), and a light depletion in HREE. Similarly as reported above for samples from surface waters, Eu strong negative anomalies are reported, while the negative Ce anomaly is similar to that reported for EMDW (figure 2).

3.1.4 Bottom layer (down to 800 m). In the deepest layer, the shale-normalized patterns are very similar to those of the second intermediate layer, with the same LREE contents of EMDW and yttrium depletion, and both MREE and HREE contents are lower than those reported in the eastern Mediterranean waters. Negative Eu anomaly values are also recognized in sampling sites close to Pantelleria Island (figure 2).

3.2 *Suspended particulate matter*

3.2.1 Surface layer (0–50 m). The shale-normalized REE distributions of SPM samples (figure 3) show a flat behaviour with positive Eu anomalies ($Eu/Eu^* > 1$) and scarce evidence of positive Ce anomalies.

3.2.2 First intermediate layer (50–200 m). In this first intermediate layer, the REE content is very similar to that in the upper layer. Sometimes slightly positive Ce anomalies can

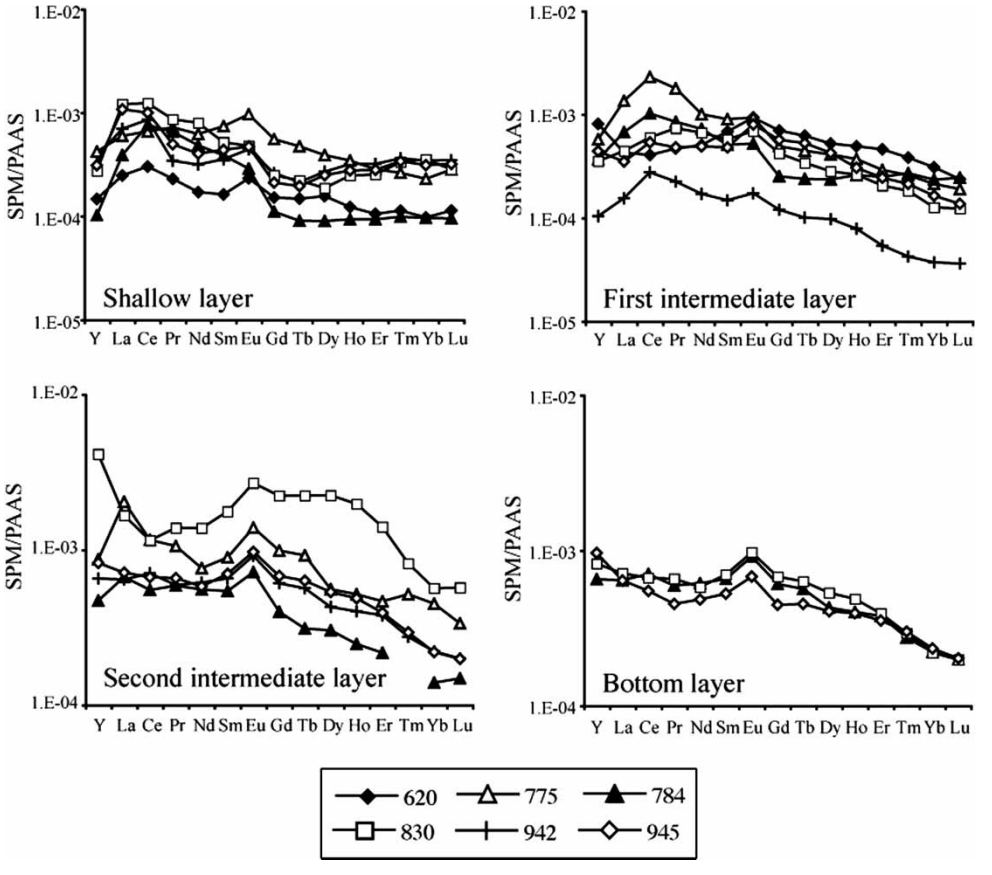

Figure 3. Shale-normalized REY patterns calculated for the average concentrations measured in SPM in the different water layers.

be detected in investigated SPM, expecially in samples with lower REE contents. Shale-normalized patterns are more regular features suggesting LREE/HREE fractionation and a flat behaviour for HREE (figure 3). Eu positive anomalies are less enhanced in this water layer.

3.2.3 Second intermediate layer (200–800 m). Shale-normalized REE patterns reported by SPM samples from this water layer illustrate the main feature of these materials:

- a general absence of positive Ce anomalies;
- the occurrence of positive Eu anomalies;
- MREE enrichments attaining a maximum with Eu, sometimes associated with a decrease in La–Ce and Yb–Lu;
- higher REE and yttrium contents recognized in sampling stations close to Pantelleria Island (figure 3).

3.2.4 Deep layer (down to 800 m). Only three sampling stations from the Pantelleria area report SPM samples from this deep layer and show very regular shale-normalized patterns, free from Ce anomalies. In contrast, Eu positive anomalies are reported in shale-normalized patterns that show a flat behaviour with scarce LREE/HREE fractionation.

4. Discussion

The main evidence that is presented in the previously reported data is that the release of trace elements from atmospheric fallout and their uptake into suspended particulate matter is the most important process to describe the fate of REY in the water columns.

If atmospheric fallout has a lithogenic origin, its REY content and distribution are driven by their charges and ionic radii because these characteristics are responsible for the trace-element distributions in minerals, allowing them to occupy the crystal lattice sites of minerals (CHarge-and-RAdius-Controlled processes).

As REY are released in the dissolved phase, they will be involved in chemical reactions, and their behaviour is basically controlled by differences in electronic external configurations (non-CHARAC processes) For instance, under these conditions, yttrium and holmium in marine environments suffer a decoupling effect due to differences in electronic external configurations between Y^{3+} and Ho^{3+}, $[Kr]4d^0$ and $[Xe]4f^{10}$, respectively. Therefore, whereas in crustal and chondritic materials, the Y/Ho ratio is clustered around 28 [28], in the marine environment the Y/Ho ratio attains values greater than 45–50 (weight/weight ratios).

Fractionation processes among LREE and HREE can be evaluated in the terms of shale normalized behaviour and using the variation of $[La/Yb]_{SN}$ ratio and in the amplitude of tetrad effects.

These are the sub-partition of REE shale normalized patterns into four 'segments' called tetrads (La–Nd, Pm–Gd, Gd–Ho, Er–Lu) [29, 30]. This evidence is called the 'tetrad effect' and is usually associated with adsorption, co-precipitation, dissolution, complexation, and/or ligand-exchange reactions [20–30]. Upward concave, W-shaped tetrad effects are observed during solid–liquid heterogeneous reactions when the covalent nature of the lanthanide ion–ligand products during the process is weaker. On the contrary, upward convex, M-shaped tetrad effects are explained in reverse mode with the increasing covalency of the REE–O bond onto a solid surface and related Racah parameters lower than in the aquo-complex. Moreover the tetrad effect can be quantified by the equation [30]:

$$t_i = \sqrt{\frac{[\mathrm{REE}]_2 \times [\mathrm{REE}]_3}{[\mathrm{REE}]_1 \times [\mathrm{REE}]_4}},$$

where t_i is the proportion of tetrad effect and $[\mathrm{REE}]_{1-4}$ denotes the normalized REE concentrations of the first, second, third, and fourth elements of a given tetrad. t_i is larger for a convex tetrad effect and smaller for a concave feature. These effects are induced by differences in the covalent character of the involved ions and represent another feature of the processes that cause Y–Ho decoupling. Usually, the amplitude of tetrad effect is evaluated according to the features of normalized concentrations only for Gd–Ho (t_3) and Er–Lu (t_4) intervals because the La–Nd (t_1) interval is affected by Ce anomalies, and the Pm–Gd (t_2) interval is not valuable for the natural occurrence on Pm.

Moreover, REY distributions in the water layers will be affected by the mass balance between the authigenic, often organic, component and the lithogenic, more chemically resistant, component of suspended particulate matter. In the present study where selective digestion procedures suitable for discriminating between the chemical signatures of these two SPM components were not carried out, the qualitative evaluation of the abundance of biogenic and lithogenic particulate components was obtained through the Cd/Sc ratio. Usually, the Cd/Al ratio is considered a useful indicator of authigenic, organic contents in suspended matter of water columns [31], with Cd being a typical 'biogenic indicator' [31–33] and Al a typical element whose fate is mainly associated with a lithogenic origin. We suggest that Sc can substitute Al to evaluate the detrital signature of SPM being less involved than Al in secondary

processes [34]. Therefore, because of these processes, recognizable signatures in terms of REE and yttrium distributions are attained in the different water layers.

In shallow water masses, the features of Y/Ho variation vs. salinity (figure 4a) suggest the occurrence of a mixing among different water masses as Modified Atlantic Water (MAW), EMDW, and LIW. With increasing depth, a preferential Y scavenging occurs, suggesting preferential yttrium removal onto montmorillonite like surfaces in the suspended particulate–water interface [35] or the occurrence of hydrothermal sources sites in the seafloor that act as sinks for dissolved yttrium [36].

Scavenging allows to a progressive decrease on Y/Ho values with depth (figure 4b) and is in agreement with measurements carried out in the S-830 sampling site whose deeper samples fall along a mixing hyperbola connecting a dissolved term with a 'normal' marine Y/Ho ratio of around 50 [37] and a deep dissolved term with an Y/Ho around 35. At the same time, the Y/Ho values measured in the SPM are clustered around 28, thus confirming the important contribution of detrital materials in the shallow waters. Furthermore, this influence, probably of Saharan origin [38], is shown by the occurrence of positive Eu anomalies in suspended particulate matter, whereas in the dissolved phase, Eu/Eu^* mainly falls close to 1 or less. This phenomenon is also influenced by the preferential incorporation of Eu (III) in newly formed carbonates through the formation of a $Eu_2(CO_3)_3$–$CaCO_3$ solid solution [39], or its biosorption in the presence of selected microorganisms [39], leaving a signature in the dissolved phase in terms of Eu/Eu^*.

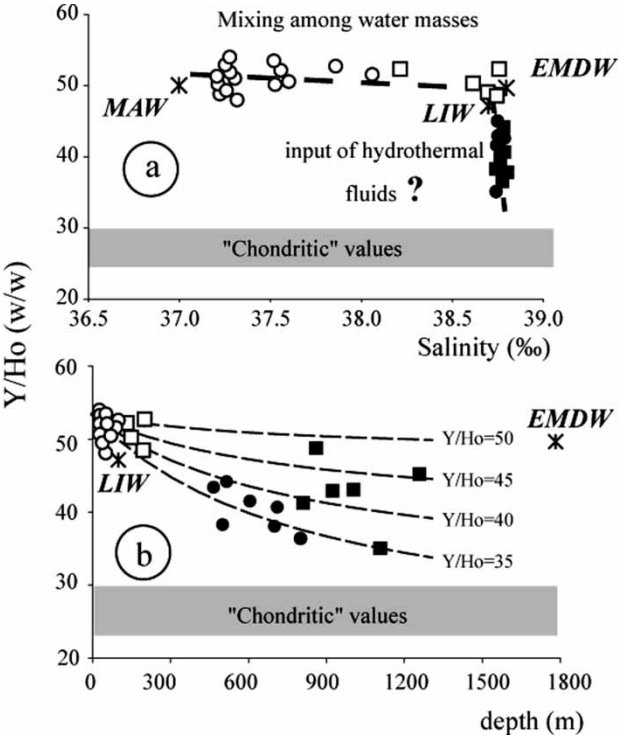

Figure 4. (a) Y/Ho ratio vs. salinity in dissolved phase. (b) Y/Ho ratio vs. sampling depth in dissolved phase. The mixing curves are calculated among a shallow end-member (Y/Ho=55; depth=10 m) and several hypothetical end-members, at a depth of 1300 m, whose Y/Ho ratios are reported along the curves for depth. Values for MAW, LIW, and EMDW are given for reference. Open circles: shallow waters; open squares: first intermediate waters; full circles: second intermediate waters; full squares: bottom waters.

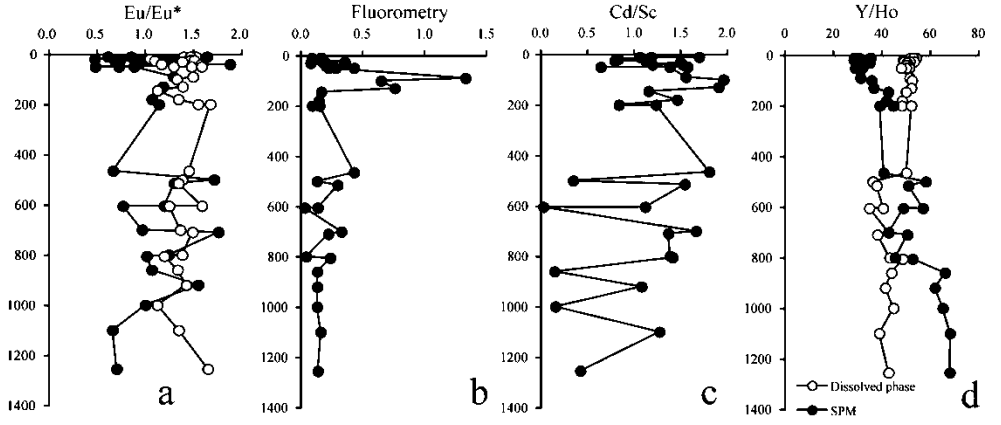

Figure 5. (a) Distributions of Eu/Eu* values calculated in the dissolved phase (open circles) and SPM (full circles). (b) Distributions of fluorometry values along the water column. (c) Behaviour of Cd/Sc values in SPM along the water depth. (d) Distribution of Y/Ho ratio measured in the dissolved phase (open circles) and SPM (full circles).

Europium uptakes is facilitated by the similarity of ionic dimension between Eu^{3+} and Ca^{2+} that allows Eu(III) to maintain the same sixfold coordination of Ca^{2+} without involving the distortions of a local calcite crystal lattice [39]. Such a process is easily responsible for the MREE enrichment reported in several foraminifera species [40] and influences the occurrence of Eu anomalies along all the water column in the dissolved phase (figure 5a).

Along the intermediate water layers, the largest productivity of water columns is recorded in terms of chlorophyll a content and is expressed as fluorometry (figure 5b). Its maxima agree also with the Cd/Sc ratio in SPM and show the same behaviour along the water depth (figure 5c). Furthermore, the covariance between Cd/Sc ratio in SPM and Fluorometry of water column demonstrate as this ratio is able to monitor the authigenic, labile fraction in suspended particulate (figure 6a). In the same layers, the covariance between Cd/Sc and $[La/Yb]_{SN}$ occurring in SPM (figure 6) suggests that lower $[La/Yb]_{SN}$ values are a signature of a low lithogenic fraction in SPM, while higher $[La/Yb]_{SN}$ values can indicate more important lithogenic contributions in SPM, as reported by Kuss *et al.* [41].

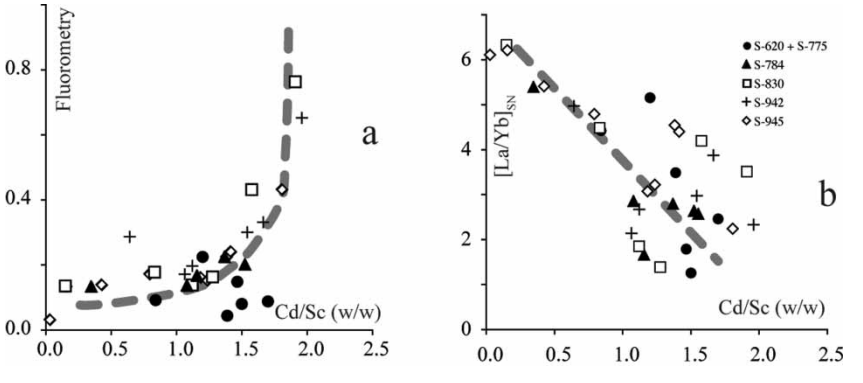

Figure 6. (a) Distributions of fluorometry values in the water columns vs. Cd/Sc ratio. (b) $[La/Yb]_{SN}$ vs. Cd/Sc values in SPM.

In deeper water layers, Y/Ho ratios progressively increase with depth, suggesting preferential yttrium scavenging onto suspended matter during the formation of an authigenic SPM fraction (figure 5d). This hypothesis disagrees with the larger affinity of REE than yttrium for SPM surfaces during simple sorption processes, and it suggests the occurrence of surface complexation reactions during which more covalent interactions are involved, and the stronger character of 'hard' Y^{3+} ion is preferred with respect to the 'softer' Ho^{3+} character [42] (figure 7). In the bottom waters Y/Ho ratios furthermore increase, suggesting the local presence of hydrothermal vent sites acting as sinks for dissolved Y [43], located at seafloor of S-830 sampling site, near the Pantelleria area.

As previously discussed, the Cd/Sc ratio is suitable for recognizing the presence of the authigenic labile fraction in SPM, but it is not a tracer clay contribution to the authigenic suspended matter. Therefore, we suggest improving this evaluation by considering both shape and amplitude of tetrad effects because:

- the REE adsorption onto the clay suspended fraction occurs only through weak interactions without tetrad effects [44];
- REE uptake onto organic matter has a M-shaped tetrad effect resulting from an inner-sphere interaction [45].

To test this hypothesis, the REE behaviour of the apparent distribution coefficients between suspended particulate and dissolved phase was calculated. Their features show that in samples showing Cd/Sc ratios less than 1.2, W-shaped tetrad effects are weak and mainly reported in both Gd–Ho and Er–Lu intervals (figure 8a). On the contrary, in SPM with Cd/Sc ratios larger than 1.2, many samples show M-shaped tetrad effects (figure 8b). Therefore, low Cd/Sc ratios in SPM indicate the presence of a lithogenic or a clay authigenic fraction, whereas larger Cd/Sc values represent an indicator of larger organic contents of the authigenic fraction of SPM, but if the suspended matter has a detrital origin, the REE behaviour of the apparent distribution coefficients should be free from any tetrad effects.

Usually the tetrad effect is observed when REE are scavenged through the formation of inner sphere complexes, such as during their adsorption on the surfaces of clay. In contrast, the tetrad effect disappears when REE are weakly sorbed as outer sphere complexes [42, 46]. Therefore, Kd behaviour suggests that REE are released by lithogenic particulates in shallow waters (M-tetrad effects), whereas their removal through the formation of weakly, outer sphere complexes occurs in deeper waters where W-tetrad effects are rare. When the hydrated ion is

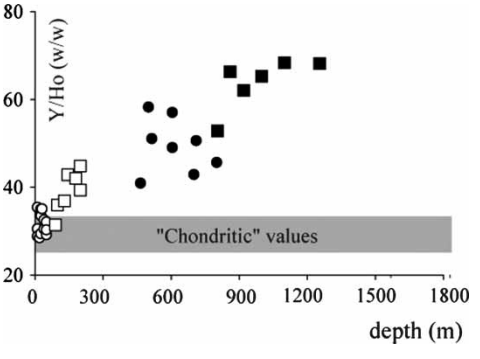

Figure 7. Y/Ho ratio vs. sampling depth in SPM. Symbols as in figure 4.

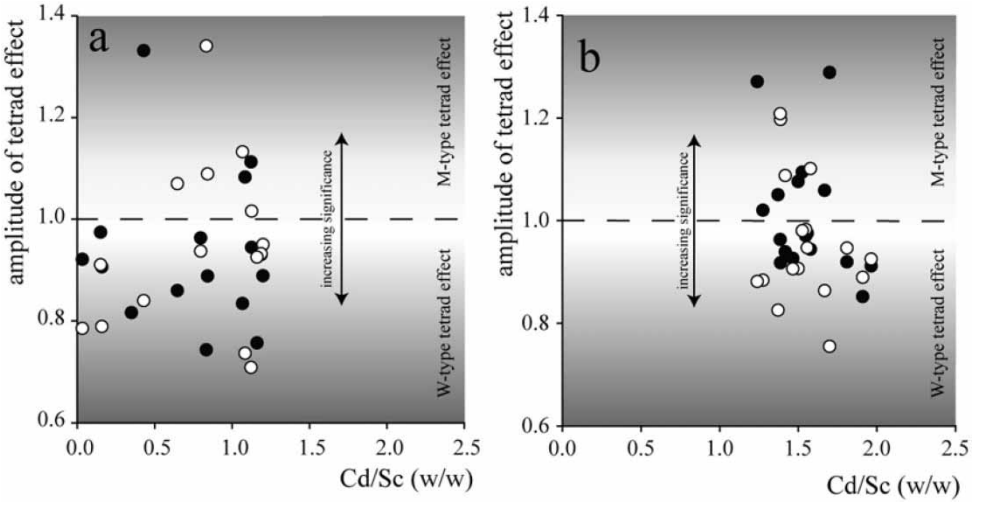

Figure 8. Amplitude of tetrad effect calculated from K_d values for Gd–Ho (t_3, open circles) and Er–Lu (t_4, full circles) intervals, according to equation (3). The gradient of the background describes the increasing significance of the values of tetrad effects according to Monecke *et al.* [30].

the main REE species in the aqueous phase, the tetrad effect is observed because the sorbed REE easily forms inner sphere complexes whose formation is accompanied by the release of hydrated water. If the main REE species are carbonate complexes, the surface complexation as REE inner-sphere complexes is more difficult in sea water, and outer-sphere complexes will be enhanced [45].

In contrast, in deep waters, REE removal occurs as weak outer sphere surface complexes, and this leads to an increase in the Y/Ho ratio in SPM due to preferential scavenging of yttrium because it is involved in stronger inner sphere surface complexes [46] (figure 5d).

5. Conclusions

The input of lithogenic materials is the most important source of lanthanides in sea water, especially in the central Mediterranean area, where riverine inputs are negligible. In the Strait of Sicily, the REY behaviour in the water masses is driven by these inputs, mixing of water masses that takes place in shallow water layers, and release-scavenging processes at the dissolved phase–suspended matter interface.

These aforementioned abilities to elucidate geochemical characteristics and processes in scawater, through the development of unique distributions of both REE and yttrium, have allowed us to identify the behaviour of several water layers in the examined area. The evaluation of the nature of suspended particulate in the water column and the mechanisms of surface complexation through stronger inner-sphere complexes were evaluated in terms of the shape of tetrad effects and the Y/Ho ration.

This study demonstrates that marine processes like water mass mixing, nutrient disposal in the water column, occurrence of hydrothermal sources in seafloor or trace element scavenging at the solid-liquid interface, can be successfully described by the combination of geochemical tracers constituted by REY distribution, tetrad effect feature and amplitute, Y/Ho and Cd/Sc rations and Eu anomaly.

References

[1] R.H. Byrne, E.R. Sholkovitz. Marine Chemistry and Geochemistry of the Lanthanides. In *The Handbook on the Physics and Chemistry of the Rare Earths*, K.A. Gschneidner, Jr, L. Eyring (Eds), Vol. 23, p. 497, Elsevier Science, Amsterdam (1996).

[2] D.S. Alibo, Y. Nozaki. Rare earth elements in seawater: Particle association, shale-normalization, and Ce oxidation. *Geochim. Cosmochim. Acta*, **63**, 363 (1999).

[3] K. Tachikawa, C. Jeandel, A. Vangriesheim, B. Dupré. Distribution of rare earth elements and neodymium isotopes in suspended particles of the tropical Atlantic Ocean (EUMELI site). *Deep Sea Res.*, **46**, 733 (1999).

[4] K.A. Quinn, R.H. Byrne, J. Schijf. Comparative scavenging of yttrium and the rare earth elements in seawater: Competitive influences of solution and surface chemistry. *Aquat. Geochem.*, **10**, 59 (2004).

[5] M. Bau, P. Dulski. Anthropogenic origin of positive gadolinium anomalies in river waters. *Earth Planet. Sci. Lett.*, **143**, 245 (1996).

[6] M.J. Greaves, H. Elderfield, E.R. Sholkovitz. Aeolian sources of rare earth elements to the Western Pacific Ocean, *Mar. Chem.*, **68**, 31 (1999).

[7] P. Censi, S. Mazzola, M. Sprovieri, A. Bonanno, B. Patti, R. Punturo, S.E. Spoto, F. Saiano, G. Alonzo. Rare earth elements distribution in seawater and suspended particulate of the Central Mediterranean Sea. *Chem. Ecol.*, **20**, 323 (2004).

[8] P. Censi, S.E. Spoto, G. Nardone, M. Sprovieri, F. Saiano, D. Ottonello, S.E. Di Geronimo. REE and yttrium distribution in mangrove coastal water systems. The western Gulf of Thailand. *Chem. Ecol.*, **21**, 255 (2005).

[9] N.H. Morley, J.D. Burton, S.P.C. Tankere, J.M. Martin. Distribution and behaviour of some dissolved trace metals in the western Mediterranean Sea, *Deep Sea Res.*, **44**, 675 (1997).

[10] Y.Y. Yoon, J.M. Martin, M.H. Cotté. Dissolved trace metals in the Western Mediterranean Sea: total concentration and fraction isolated by C18 Sep-Pak technique. *Mar. Chem.*, **66**, 129 (1999).

[11] S.W. Fowler, T.F. Hamilton, R.D. Peinert, J. La Rosa, J.-L Teyssie. The vertical flux of Rare Earth Elements in the Northwestern Mediterranean. *Wat. Pollut. Res. Rep.*, **28**, 401 (1992).

[12] M.J. Greaves, M. Rudnicki, H. Elderfield. Rare earth elements in the Mediterranean Sea and mixing in the Mediterranean outflow. *Earth Planet. Sci. Lett.*, **103**, 169 (1991).

[13] A.J. Thomas, C. Guieu, J.M. Martin. Comment on 'Rare earth elements in the Mediterranean Sea and mixing in the Mediterranean outflow' by M.J. Greaves, M. Rudnicki and H. Elderfield. *Earth Planet. Sci. Lett.*, **121**, 655 (1995).

[14] P.M. Saager, J. Schijf J.W. De Baar. Trace-metal distributions in seawater and anoxic brines in the eastern Mediterranean Sea. *Geochim. Cosmochim. Acta*, **57**, 1419 (1993).

[15] J. Schijf J.W. De Baar. Rare earth elements through the Bosporus: the Black Sea as a net source of REEs to the Mediterranean Sea. *Geochim. Cosmochim. Acta*, **59**, 3503 (1995).

[16] M. Bau, P. Moller, P. Dulski. Yttrium and lantanides in eastern Mediterranean seawater and their fractionation during redox cycling, *Mar. Chem.*, **56**, 123 (1997).

[17] R. Arraes-Mescoff, M. Roy-Barman, M.L. Coppola, M. Souhaut, K. Tachikawa, C.R. Jeandel, R. Sempéré, C. Yoro. The behaviour of Al, Mn, Ba, Sr, REE and Th isotopes during *in vitro* degradation of large marine particles. *Mar. Chem.*, **73**, 1 (2001).

[18] I. Finetti. Geophysical study of the Sicily channel rift zone, *Boll. Geo¢ s. Teor. Appl.*, **26**, 101 (1984).

[19] C.D., Reuther, G.H. Eisbacher. Pantelleria rift-crustal extension in a convergent intraplate setting, *Geol. Rundsch.*, **74**, 585 (1985).

[20] M. Boccaletti, G. Cello, L. Tortorici. Transtensional tectonics in the Sicily Channel, *J. Struct. Geol.*, **9**, 869 (1987).

[21] F. Parello, P. Allard, W. D'Alessandro, C. Federico, P. Jean-Baptiste, O. Catani. Isotope geochemistry of Pantelleria volcanic fluids, Sicily Channel rift: a mantle volatile end-member for volcanism in southern Europe. *Earth Planet. Sci. Lett.*, **180**, 325 (2000).

[22] P. Censi, S. Mazzola, B. Patti, F. Saiano, M. Sprovieri, G. Alonzo, S.E. Spoto. Trace element distributions in the Straits of Sicily (Central Mediterranean Sea). I. Evidences of rock–water interactions and pollution. *Periodico di Mineralogia*, **71**, 255 (2002).

[23] F. FengFu, K. Shinotsuka, M. Ebihara, T. Akagi. Distribution ratio of dissolved and particulate REE in surface coastal waters. *Geochem. J.*, **31**, 303 (1997).

[24] P. Möller, P. Dulski, J. Luck. Determination of rare earth elements in seawater by inductively coupled plasma-mass spectrometry. *Spectrochim. Acta*, **47B**, 1379 (1992).

[25] A.J. Paulson. The effects of flow rate and pre-treatment on the analyses of trace metals in estuarine and coastal seawater by Chelex-100. *Anal. Chem.*, **58**, 183 (1986).

[26] P. Censi, S.E. Spoto, F. Saiano, G. Nardone, M. Sprovieri, S. Mazzola, R. Punturo, D. Ottonello, S.E. Di Geronimo. Heavy metal contents in coastal water systems. A case of study in the Northwestern Gulf of Thailand. *Chemosphere*, **64**, 1167–1176 (2006).

[27] S.R. Taylor, S.M. McLennan. *The Continental Crust: Its Composition and Evolution*, Blackwell Scientific, Oxford (1985).

[28] M. Bau. Controls on the fractionation of isovalent trace elements in magmatic and aqueous systems: evidence from Y/Ho, Zr/Hf, and lanthanide tetrad effect. *Contrib. Miner. Petrol.*, **123**, 323 (1996).

[29] A. Masuda O. Kawakami, Y. Dohomoto, T. Takenaka. Lanthanide tetrad effects in nature: two mutually opposite types, W and M. *Geochem. J.*, **21**, 119 (1987).

[30] T. Monecke, U. Kempe, J. Monecke, M. Sala, D. Wolf. Tetrad effect in rare earth element distribution patterns: A method of quantification with application to rock and mineral samples from granite-related rare metal deposits. *Geochim. Cosmochim. Acta*, **66**, 1185 (2002).
[31] J. Kuss, K. Kremling. Spatial variability of particle associated trace elements in near-surface waters of the North Atlantic (30° N/60° W to 60° N/2° W), derived by large volume sampling. *Mar.Chem.* **68,** 71 (1999).
[32] K.W. Bruland. Trace elements in sea-water. In *Chemical Oceanography*, Vol. 8, J.P. Riley, R. Chester (Eds), pp. 157–220, Academic Press, London (1983).
[33] S.W. Fowler, G.A. Knauer. Role of large particles in the transport of elements and organic compounds through the oceanic water column. *Prog. Oceanogr.*, **16**, 147 (1986).
[34] F.E. Grousset C.R. Quetel, B. Thomas, O.F.X. Donard, C.E. Lambert, F. Guillard, A. Monaco. Anthropogenic vs. lithogenic origins of trace elements (As, Cd, Pb, Rb, Sb, Sc, Sn, Zn) in water column particles: northwestern Mediterranean Sea. *Mar. Chem.*, **48**, 291 (1995).
[35] E.J. Elzinga, R.J. Reeder, S.H. Withers, R.E. Peale, R.A. Mason, K.M., W.P. Hess. EXAFS study of rare-earth element coordination in calcite. *Geochim. Cosmochim. Acta*, **66,** 2875 (2002).
[36] Y. Takahashi, A. Tada, H. Shimizu. Distribution patterns of rare earth ions between water and Montmorillonite and its relation to the sorbed species of the ions. *Anal. Sci.*, **20B**, 1301 (2004).
[37] Y. Nozaki, J. Zhang, H. Amakawa. The fractionation between Y and Ho in the marine environment. *Earth Plan. Sc. Lett.*, **148**, 329 (1997).
[38] E. Molinaroni. Mineralogical characterization of Saharan dust with a view to its final destination in Mediterranean sediments. In *The Impact of Desert Dust Across the Mediterranean*, S. Guerzoni, R. Chester (Eds), pp. 153–162, Kluwer Academic Press, Dordrecht, Netherlands (1996).
[39] L.Z. Lakshtanov, S.L.S. Stipp. Experimental study of europium (III) coprecipitation with calcite. *Geochim. Cosmochim. Acta*, **68**, 819 (2004).
[40] B.A. Haley, G.P. Klinkhammer, A.C. Mix. Revisiting the rare earth elemento in foraminiferal tests. *Earth Planet. Sci. Lett.*, **239**, 79 (2005).
[41] J. Kuss, C.-D. Garbe-Schonberger, K. Kremling. Rare earth elements in suspended particulate material of North Atlantic surface waters. *Geochim. Cosmochim. Acta*, **65**, 187 (2001).
[42] F. Coppin, G. Berger, A. Bauer, S. Castet, M. Loubet. Sorption of lanthanides on smectite and kaolinite. *Chem. Geol.*, **182**, 57 (2002).
[43] M. Bau, P. Dulski. Comparing yttrium and rare earths in hydrothermal fluids from the Mid-Atlantic Ridge: implications for Y and REE behaviour during near-vent mixing and for the Y/Ho ratio of Proterozoic seawater. *Chem. Geol.*, **155**, 77 (1999).
[44] Z. Tao, X. Wang, Z. Guo, T. Chu. Is there a tetrad effect in the adsorption of lanthanides (III) at solid–water interfaces? *Colloids Surf. A*, **251**, 19 (2004).
[45] Y. Takahashi, X. Chatellier, K.H. Hattori, K. Kato, D. Fortin. Adsorption of rare earth elements onto bacterial cell walls and its implication for REE sorption onto natural microbial mats. *Chem. Geol.*, **219**, 53 (2005).
[46] Y. Takahashi, A. Tada, H. Shimizu. Distribution patterns of rare earth ions between water and montmorillonite and its relation to the sorbed species of the ions. *Anal. Sci.*, **20B**, 1301 (2004).